

Brown-fat paucity due to impaired BMP signalling induces compensatory browning of white fat

Tim J. Schulz¹†, Ping Huang², Tian Lian Huang¹, Ruidan Xue^{1,3}, Lindsay E. McDougall¹, Kristy L. Townsend¹, Aaron M. Cypess¹, Yuji Mishina⁴, Emanuela Gussoni² & Yu-Hua Tseng^{1,5}

Maintenance of body temperature is essential for the survival of homeotherms. Brown adipose tissue (BAT) is a specialized fat tissue that is dedicated to thermoregulation1. Owing to its remarkable capacity to dissipate stored energy and its demonstrated presence in adult humans²⁻⁵, BAT holds great promise for the treatment of obesity and metabolic syndrome1. Rodent data suggest the existence of two types of brown fat cells: constitutive BAT (cBAT), which is of embryonic origin and anatomically located in the interscapular region of mice; and recruitable BAT (rBAT), which resides within white adipose tissue (WAT)⁶ and skeletal muscle⁷, and has alternatively been called beige⁸, brite⁹ or inducible BAT¹⁰. Bone morphogenetic proteins (BMPs) regulate the formation and thermogenic activity of BAT¹⁰⁻¹². Here we use mouse models to provide evidence for a systemically active regulatory mechanism that controls whole-body BAT activity for thermoregulation and energy homeostasis. Genetic ablation of the type 1A BMP receptor (Bmpr1a) in brown adipogenic progenitor cells leads to a severe paucity of cBAT. This in turn increases sympathetic input to WAT, thereby promoting the formation of rBAT within white fat depots. This previously unknown compensatory mechanism, aimed at restoring total brown-fat-mediated thermogenic capacity in the body, is sufficient to maintain normal temperature homeostasis and resistance to diet-induced obesity. These data suggest an important physiological cross-talk between constitutive and recruitable brown fat cells. This sophisticated regulatory mechanism of body temperature may participate in the control of energy balance and metabolic disease.

It has recently become clear that cBAT shares a common developmental ancestry with skeletal muscle^{13,14}, whereas rBAT, localized within white fat or skeletal muscle, is derived from a non-myogenic lineage^{10,13}. Lineage-tracing experiments have also revealed that cBAT arises from progenitors located in the embryonic dermomyotome¹⁵ that express the myogenic markers Pax7 and Myf5 (refs 13, 16). Thus, we generated a mouse model lacking BMPR1A in all cells descending from the Myf5⁺ lineage (Myf5-BMPR1A-KO). No apparent changes in morphology, proliferation or apoptosis were observed during early embryonic stages (Supplementary Figs 1 and 2). Histological evidence of reduced cBAT formation in Myf5-BMPR1A-KO mice was observed at embryonic day (E)16.5 and persisted until after birth (postnatal day (P)1; Fig. 1a-c). cBAT arises from highly proliferative fibroblasts during late gestational stages¹⁷. At E16.5, developing cBAT stains strongly for the proliferation marker Ki67, which was markedly decreased in Myf5-BMPR1A-KO embryos (Fig. 1d and Supplementary Fig. 2b, d). Apoptosis levels were unchanged in knockout mice compared to controls throughout embryogenesis (Supplementary Fig. 2c), suggesting that reduced proliferation occurring before or around E16.5 is responsible for the defective formation of cBAT in knockout animals.

Myf5-BMPR1A-KO mice were born runted and stayed smaller throughout life (Fig. 1e, f). Importantly, the reduction of cBAT mass remained highly significant in adult mice (Fig. 1g, h). Despite this, the gene-expression pattern of the residual cBAT appeared normal, apart from a moderate reduction of Bmpr1a gene expression (Supplementary Fig. 3). The sizes of interscapular WAT (iWAT) and retroperitoneal WAT (rWAT)—two white-fat depots that contain subpopulations of cells from the Myf5⁺ lineage¹⁸—were also reduced in the knockout mice (Supplementary Fig. 4a). Gene expression in iWAT showed a trend towards reduced expression of BAT genes, but there were no changes in the expression of general white adipogenic genes (Supplementary Fig. 4b). Subcutaneous WAT (sWAT) and epididymal WAT (eWAT), both mostly originating from a Myf5⁻ lineage¹⁸, were not decreased in size and expressed normal levels of all type-1 BMP receptors (Fig. 1g, h and Supplementary Fig. 3a–c). Expression of *Bmpr1a* in skeletal muscle, on the other hand, was reduced by >95% (Supplementary Fig. 3a). Upon normalization to body weight, we found that limb skeletal muscle size was unchanged, whereas the function of myogenic progenitors was altered (P.H. and E.G., unpublished data). Thus, loss of BMP signalling in Myf5-expressing cells specifically targets the formation of cBAT. During embryogenesis, MyoD⁺ progenitors emerge after the Myf5⁺ progenitors¹⁹. MyoD-Cre-driven Bmpr1a knockout mice showed completely normal development of cBAT and WAT depots (Supplementary Fig. 5), suggesting that the developmental divergence between myogenic and brown adipogenic progenitors takes place before the emergence of MyoD⁺ progenitors, or that BMPR1A is not required for cBAT formation during this particular developmental

A very similar phenotype was observed in a second mouse model with conditional deletion of *Bmpr1a* in all types of adipocytes (FABP4-BMPR1A-KO). Loss of *Bmpr1a* led to a specific paucity of cBAT as well as WAT-resident rBAT (Supplementary Fig. 6). Because the FABP4-Cre driver is active at later adipogenic stages compared to Myf5-Cre, we conclude that signalling through BMPR1A is essential also for later stages of brown adipogenesis.

Next, we isolated progenitors from either Myf5⁻ sWAT or Myf5⁺ cBAT to test their cell-autonomous ability to produce brown adipocytes¹⁰. Cells derived from sWAT differentiated normally (Supplementary Fig. 7). By contrast, the frequency and ability of cBAT-derived Myf5⁺/Sca1⁺/CD31⁻ (Sca1 also known as Ly6a; CD31 also known as Pecam1) progenitors to differentiate into mature brown adipocytes was significantly reduced (Fig. 2a, b). We therefore generated brown preadipocytes from cBAT completely lacking BMPR1A (Supplementary Fig. 8a, b). Loss of *Bmpr1a* resulted in a marked inhibition of differentiation (Fig. 2c), and reduced ability to respond to BMP7-induced phosphorylation of SMAD and p38-mitogen-activated protein kinase (p38MAPK; also known as MAPK14)²⁰, which are downstream targets

¹Section on Integrative Physiology and Metabolism, Joslin Diabetes Center, Harvard Medical School, Boston, Massachusetts 02215, USA. ²Program in Genomics and Division of Genetics, Boston Children's Hospital, Harvard Medical School, Boston, Massachusetts 02115, USA. ³Division of Endocrinology and Metabolism, Huashan Hospital, Shanghai Medical College, Fudan University, Shanghai 200032, China. ⁴Department of Biologic and Materials Sciences, School of Dentistry, University of Michigan, Ann Arbor, Michigan 48109, USA. ⁵Harvard Stem Cell Institute, Harvard University, Cambridge, Massachusetts 02138, USA. [†]Present address: Research Group Adipocyte Development, German Institute of Human Nutrition, Potsdam-Rehbrücke, Nuthetal 14558, Germany.

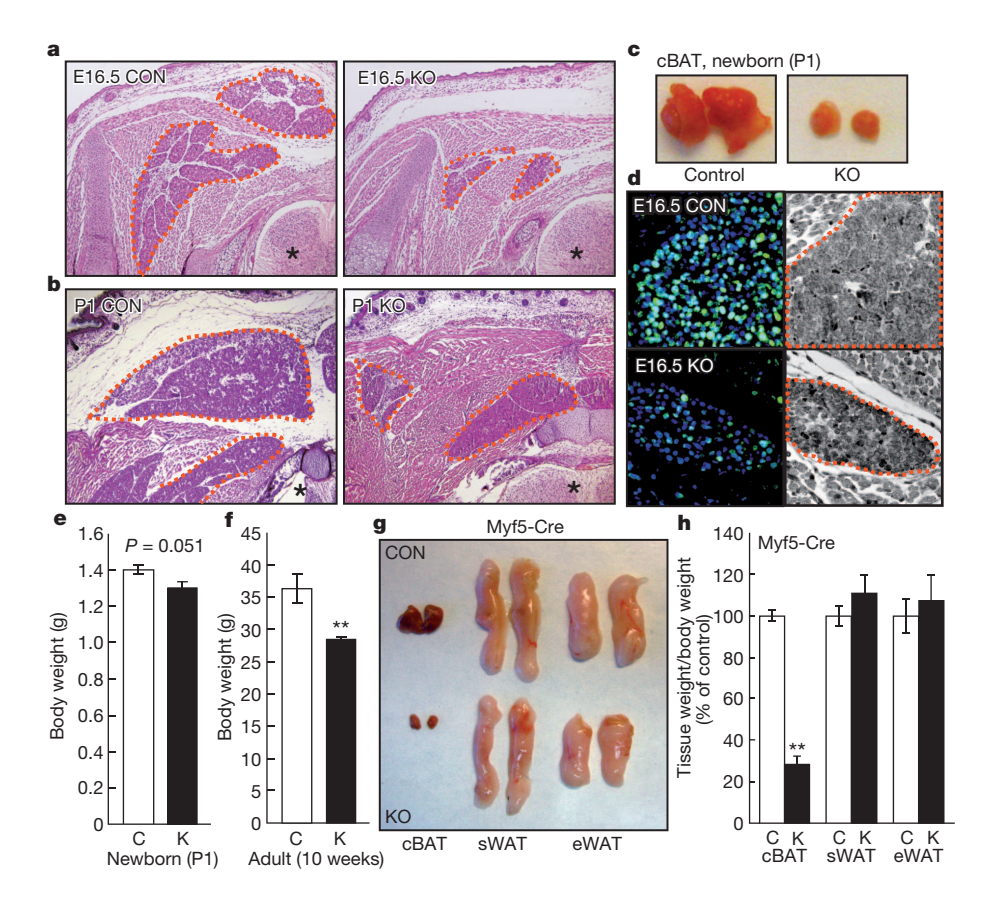


Figure 1 | Loss of Bmpr1a impairs cBAT formation by decreasing embryonic progenitor proliferation. a, b, Haematoxylin and eosin staining of interscapular sections at embryonic stage E16.5 and in newborns (P1). Photographs (original magnification, ×100) of the same anatomical location of transversal sections were acquired for control (CON) and Myf5-BMPR1A-KO mice (KO). Asterisks indicate spinal cord, orange lines indicate brown fat. c, Macroscopic images of cBAT of P1 newborns. d, Ki67 immunofluorescence (green) of cBAT at E16.5 and co-localization with nuclear 4',6-diamidino-2phenylindole (DAPI) stain (blue, left panels; analysis of Ki67⁺ nuclei in Supplementary Fig. 1d), and light microscopy of the same area (right panels: original magnification, ×400). Orange lines indicate brown fat. e, f, Body weight analysis of control (C) and Myf5-BMPR1A-KO (K) mice from P1 newborns (e; control: n = 12; knockout: n = 4) and adult mice (\mathbf{f} ; n = 6). \mathbf{g} , \mathbf{h} , Analysis of cBAT, sWAT and eWAT weights after normalization to body weight (n = 13). All data are presented as mean ± standard error of the mean (s.e.m.) Asterisks denote significant differences between genotypes: **P < 0.01.

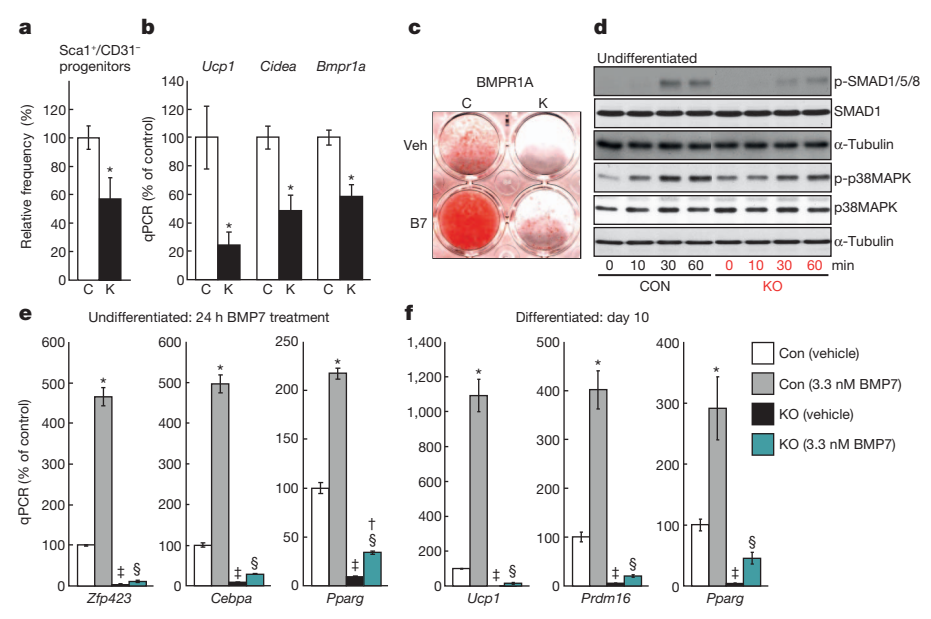


Figure 2 | Ablation of *Bmpr1a* in brown pre-adipocytes derived from the Myf5⁺ lineage inhibits differentiation. a, Relative frequency of Sca1⁺/ CD31⁻/CD11b⁻/CD45⁻ adipogenic progenitors of the Myf5-Cre(YFP)⁺ lineage in cBAT after normalization to tissue weight (n=6). White bars indicate cells isolated from control mice (C), black bars indicate Myf5-BMPR1A-KO cells (K). b, Quantitative polymerase chain reaction (qPCR) analysis of *Ucp1*, *Cidea* and *Bmpr1a* messenger RNAs in fluorescence-activated cell sorting (FACS)-purified primary progenitors from cBAT after adipogenic differentiation (n=3). Asterisks denote significant differences between genotypes: *P< 0.05. c, Triglyceride-specific Oil-Red-O staining of differentiated control (C) or BMPR1A-deficient (K) immortalized preadipocyte cell lines pretreated with vehicle (Veh) or BMP7 (B7). d, Western blot of phospho (p)-SMAD1/5/8, basal SMAD1, corresponding α -tubulin,

phospho-p38MAPK, basal p38MAPK, and corresponding α -tubulin in undifferentiated control (CON) and pre-adipocytes lacking BMPR1A (KO) following exposure to BMP7 for 10, 30 and 60 min. Representative blots from three independent experiments are shown. **e**, qPCR of *Zfp423*, *Cebpa* and *Pparg* in undifferentiated brown pre-adipocytes after 24 h exposure to BMP7. **f**, qPCR of *Ucp1*, *Prdm16* and *Pparg* isolated from mature brown adipocytes. Pre-adipocytes were treated with BMP7 for 3 days, followed by 7-day differentiation. All experiments were performed in triplicate and are presented as mean \pm s.e.m. **e**, **f**, Statistically significant differences as determined by analysis of variance (ANOVA; P < 0.05) were: control (vehicle) versus control (BMP7) (*); KO (vehicle) versus KO (BMP7) (†); control (vehicle) versus KO (vehicle) (‡); and control (BMP7) versus KO (BMP7) (§).

of BMP signalling (Fig. 2d). This led to a concomitant decrease in the expression of key adipogenic transcription factors zinc-finger protein 423 (Zfp423)²¹, CCAAT/enhancer-binding protein α (Cebpa) and peroxisome-proliferator-activated receptor γ (*Pparg*)²² in undifferentiated pre-adipocytes (Fig. 2e). After adipogenic differentiation, BMPR1Aknockout cells showed severely reduced expression of BAT markers Ucp1, PR-domain containing 16 (Prdm16)13 and Pparg (Fig. 2f), even in the presence of BMP7. Aside from BMPR1A, BMPR1B and activin A receptor, type 1 (ACVR1) are the other two major type-1 BMP receptors²⁰. Whereas cBAT developed normally in whole-body BMPR1B-knockout mice (Supplementary Fig. 9a, b), deletion of Acvr1 in the Myf5⁺ lineage resulted in a severe reduction of cBAT mass (Supplementary Fig. 9c, d), indicating that both ACVR1 and BMPR1A are essential for development of cBAT. Accordingly, pre-adipocytes lacking Acvr1 showed a somewhat milder phenotype compared to BMPR1Adeficient cells, whereas in double-knockout cells, brown adipogenesis was completely abolished (Supplementary Fig. 8c-g).

As BAT has a key role in thermoregulation, one would anticipate that the Myf5-BMPR1A-KO mice would have reduced body temperature as a consequence of impairment in cBAT development. Indeed, newborn Myf5-BMPR1A-KO mice, with their unfavourable surfaceto-volume ratio, showed a significant reduction in body temperature (Fig. 3a, b). This reduction in body temperature was, surprisingly, no longer present in adult Myf5-BMPR1A-KO mice maintained at normal ambient temperatures of 22 °C (Fig. 3c, bars labelled 22 °C), indicating a compensatory mechanism that restored thermogenic capacity. Non-shivering thermogenesis is a critical response to prolonged cold exposure in order to maintain body temperature²³. When exposed to acute and chronic cold challenges, control mice were able to quickly return to normal body temperature after 48 h of cold exposure, suggesting rapid activation of non-shivering thermogenesis via cBAT, and possibly other short-term measures such as muscle shivering, which are less pronounced in newborn mice. By contrast, Myf5-BMPR1A-KO mice showed a reduction in body temperature after 2 h and 48 h of cold exposure at 5 °C, presumably due to the paucity of cBAT (Fig. 3c, bars labelled 5 °C/2 h and 5 °C/48 h), as we did not observe any abnormal behaviour, such as increased shivering, under cold exposure. Despite this, body temperature in Myf5-BMPR1A-KO mice returned to normal after prolonged cold exposure (that is, 11 days), strongly suggesting an adaptive recruitment of rBAT to cope with lower ambient temperatures (Fig. 3c, bars labelled 5 °C/11 d). Accordingly, knockout animals showed a marked increase in UCP1 protein expression in sWAT (Fig. 3d and Supplementary Fig. 10). This browning effect could be further enhanced in sWAT, and induced in eWAT, by administration of the β3-adrenergic receptor agonist CL-316,243, as indicated by significantly increased expression of BAT markers Ucp1 and celldeath-inducing DFFA-like effector a (Cidea) in Myf5-BMPR1A-KO mice (Fig. 3e-h), as well as by increased emergence of multilocular UCP1⁺ adipocytes in WAT (Fig. 3i, j).

rBAT is sensitive to inductive factors, such as BMP7 (refs 10, 11), BMP8b12, fibroblast growth factor 21 (FGF21)24 and the myokine irisin²⁵ (which is the processed and secreted form of the *Fndc5* gene product), among others. However, gene expression analysis revealed no changes in any of these (Supplementary Fig. 11), suggesting that the compensatory browning is not mediated by these factors. Because thermogenesis is rigorously controlled by the sympathetic nervous system^{26,27}, we quantified sympathetic input to white fat in Myf5-BMPR1A-KO mice. Staining for tyrosine hydroxylase was significantly increased in sWAT of knockout mice (Fig. 3k, 1). Moreover, circulating levels of noradrenaline were also significantly elevated in knockout mice, suggesting that increased sympathetic input may contribute to the browning of WAT in Myf5-BMPR1A-KO mice (Fig. 3m). Additionally, cold-exposed Myf5-BMPR1A-KO mice showed normal noradrenaline-induced thermogenic capacity (Fig. 3n and Supplementary Fig. 12), and thus possess a sufficient ability to compensate for loss of cBAT. These findings suggest that both types of brown fat may possess

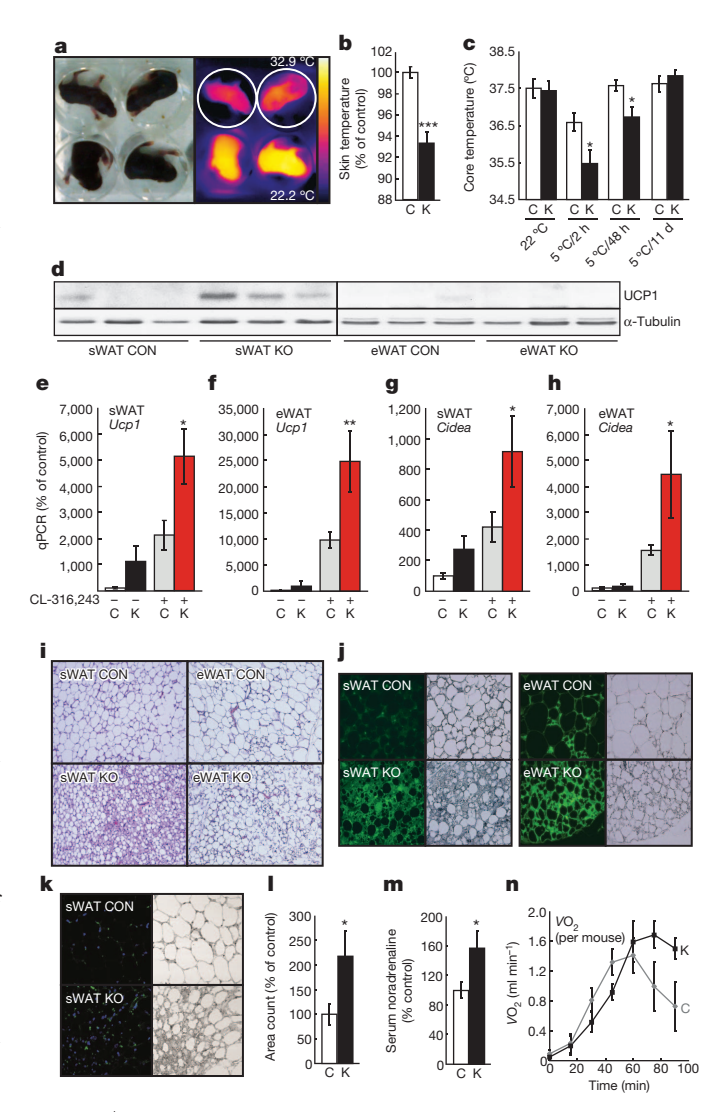


Figure 3 | Specific ablation of cBAT results in a compensatory response of increased browning by enhanced sympathetic input to WAT.

a, Photographic (left) and infrared (right) images of P4-P6 newborns. Knockout pups are indicated by white circles. b, Quantification of average skin surface temperature from infrared images. White bars indicate control mice (C), black bars indicate Myf5-BMPR1A-KO mice (K; control: n = 12; knockout: n = 10). c, Body core temperature of adult control and Myf5-BMPR1A-KO mice. Measurements were performed at room temperature (22 °C; control: n = 11; knockout: n = 10), and after 2 h (n = 5), 48 h (control: n = 7; knockout: n = 6) and 11 days (control: n = 7; knockout: n = 6) of cold exposure (5 °C). **d**, Western blot analysis of UCP1 in sWAT and eWAT. e, f, qPCR of Ucp1 gene expression in sWAT (e) and eWAT (f). Grey bars indicate controls after administration of β3-adrenergic agonist CL-316,243 (1 mg kg⁻¹ body weight) for 10 days, red bars indicate CL-316,243-injected Myf5-BMPR1A-KO mice (n = 7; applies to all panels). **g**, **h**, qPCR of *Cidea* in sWAT (g) and eWAT (h). i, Haematoxylin and eosin staining showing morphology of sWAT and eWAT after administration of CL-316,243 (original magnification, ×200). j, UCP1 immunofluorescence of sWAT and eWAT after administration of CL-316,243 (original magnification, ×400). Left panels show UCP1 immunofluorescence (green), right panels show light microscope image of the same area. k, l, Tyrosine hydroxylase immunofluorescence and quantification of tyrosine-hydroxylase-positive nerve fibres in sWAT after administration of CL-316,243 (original magnification, $\times 400$) (n = 3). **m**, Serum levels of noradrenaline (n = 8). **n**, Time course of noradrenalineinduced oxygen consumption in mice maintained at 5 °C for 8 days (grey line, control; black line, knockout; n = 5). All data are presented as mean \pm s.e.m. Asterisks denote significant differences between genotypes: *P < 0.05; **P < 0.01; ***P < 0.001.

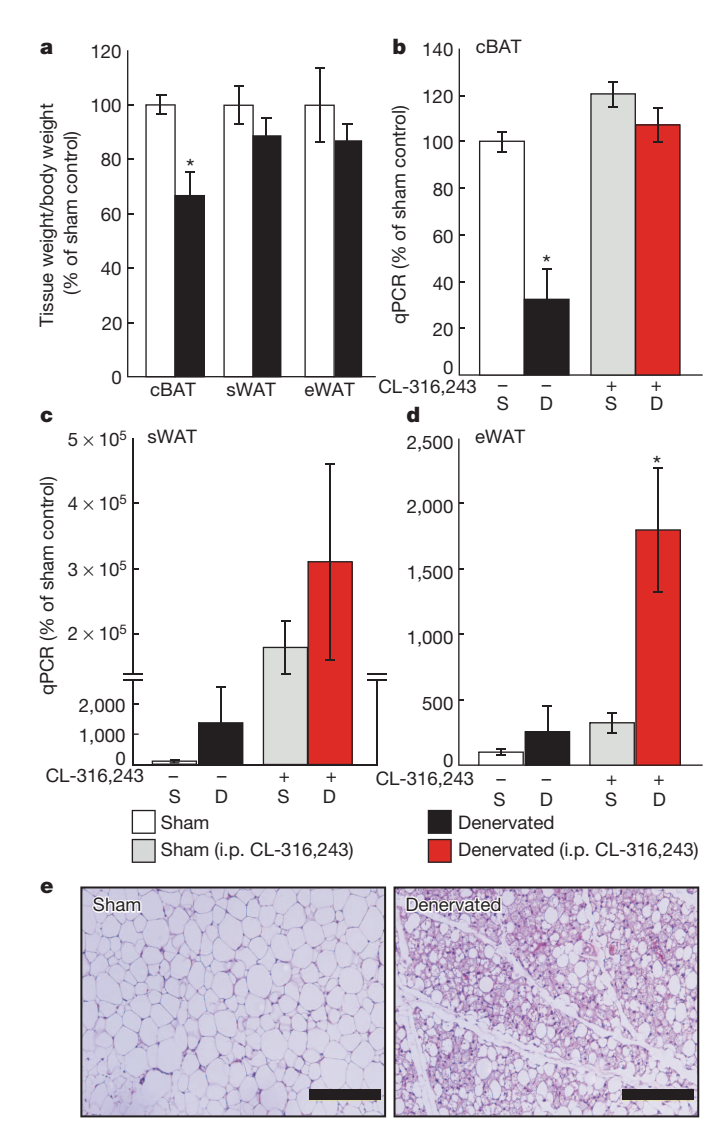


Figure 4 | Loss of sympathetic innervation causes atrophy of cBAT and compensatory browning of white fat. a, Tissue weight of cBAT, sWAT and eWAT normalized to body weight in sham-operated mice (white bars) and mice after surgical denervation of cBAT (black bars). b–d, qPCR of *Ucp1* in cBAT (b), sWAT (c) and eWAT (d) of control mice, denervated mice, controls (grey bars) or denervated (red bars) mice injected with CL-316,243. S, sham-operated mice; D, surgically denervated mice. i.p., intraperitoneal. e, Haematoxylin and eosin staining of sWAT from sham-operated and cBAT-denervated mice after CL-316,243 injections. Scale bar, 100 μ m. All data are presented as mean \pm s.e.m. (n=4). Asterisks denote significant differences between denervation and respective control groups: *P< 0.05 as determined by ANOVA.

similar capacities for thermoregulation if maximally stimulated. Whereas cBAT is essential during acute cold challenges, compensatory rBAT in the knockout mice with severe paucity of cBAT has a critical role in maintaining normal body temperature, especially during long-term cold exposure. In accordance with these findings, Myf5-BMPR1A-KO animals were resistant to diet-induced obesity, even under obesity-promoting thermoneutrality conditions, where mice no longer require thermogenesis to maintain body temperature²⁸ (Supplementary Fig. 13).

To determine whether the effect of compensatory browning is also present in other models of cBAT atrophy and independent of genetic intervention that could also affect skeletal muscle, we surgically interrupted innervation of cBAT in wild-type mice. Denervation of cBAT resulted in a significant decrease of cBAT size and a 68% reduction of Ucp1 expression in cBAT (P = 0.0029; Fig. 4a, b). As in

Myf5-BMPR1A-KO mice, atrophy of cBAT resulted in increased recruitment of brown adipocytes in WAT (Fig. 4c–e), thus reinforcing the notion of a systemic mechanism that regulates total BAT-mediated thermogenic capacity.

It has been documented before that surgical removal of the interscapular depot of cBAT causes activation of the remaining depots of cBAT²⁹. We used both genetic and surgically generated models of cBAT paucity to demonstrate the existence of a physiological mechanism to ensure thermoregulation by compensatory browning of WAT. This type of BAT may be more closely related to that found in adult humans8. The system inducing formation of rBAT seems to involve cBAT-brain and brain-WAT communication that is mediated, at least in part, by the sympathetic nervous system. Interestingly, obesity resistance in mice appears to be mostly related to browning of white fat, rather than adaptive thermogenesis of cBAT³⁰, altogether suggesting that rBAT is a key contributor to metabolic health. The findings presented here suggest that any therapeutic approach involving rBAT must take into account the tight regulation of total-BAT-mediated thermogenic capacity and systemic energy metabolism at both peripheral and possibly also central levels. Targeting these mechanisms, for instance by modifying BMP signalling to regulate BAT mass and activity, could be a feasible approach to develop obesity therapies.

METHODS SUMMARY

Animal models. For conditional knockouts, strains expressing Cre recombinase under the control of *Myf5*, *Myod* or fatty-acid-binding protein 4 (*Fabp4*) promoters were crossed to mice carrying floxed alleles for *Bmpr1a* or *Acvr1* (Myf5-Cre only). For some experiments, Myf5-BMPR1A-KO mice were crossed to a Rosa26-YFP reporter strain. For *Bmpr1b*, a strain with whole-body gene deletion was used. Denervation of cBAT in male, wild-type C57BL/6 mice was performed by isolating and removing a portion of about 1–2 mm from the intercostal nerve bundles innervating both lobes of the interscapular cBAT.

Thermal imaging of skin-surface temperature. Measurement of skin temperature was performed using a thermal imaging camera (T300 InfraRed Camera; FLIR Systems) on newborn mice at ages P4–P6, before onset of hair growth. Statistical analysis. Results are expressed as mean \pm s.e.m. Differences between two groups were assessed using unpaired two-tailed Student's t-test or U-Mann-Whitney test. Data involving more than two groups were assessed by ANOVA.

Full Methods and any associated references are available in the online version of the paper.

Received 23 May 2012; accepted 29 January 2013. Published online 13 March 2013.

- Cannon, B. & Nedergaard, J. Metabolic consequences of the presence or absence of the thermogenic capacity of brown adipose tissue in mice (and probably in humans). *Int. J. Obes. Lond.* 34 (suppl. 1), S7–S16 (2010).
- Cypess, A. M. et al. Identification and importance of brown adipose tissue in adult humans. N. Engl. J. Med. 360, 1509–1517 (2009).
- Nedergaard, J., Bengtsson, T. & Cannon, B. Unexpected evidence for active brown adipose tissue in adult humans. Am. J. Physiol. Endocrinol. Metab. 293, E444–E452 (2007)
- van Marken Lichtenbelt, W. D. et al. Cold-activated brown adipose tissue in healthy men. N. Engl. J. Med. 360, 1500–1508 (2009).
- Virtanen, K. A. et al. Functional brown adipose tissue in healthy adults. N. Engl. J. Med. 360, 1518–1525 (2009).
- Guerra, C., Koza, R. A., Yamashita, H., Walsh, K. & Kozak, L. P. Emergence of brown adipocytes in white fat in mice is under genetic control. Effects on body weight and adiposity. J. Clin. Invest. 102, 412–420 (1998).
- Almind, K., Manieri, M., Sivitz, W. I., Cinti, S. & Kahn, C. R. Ectopic brown adipose tissue in muscle provides a mechanism for differences in risk of metabolic syndrome in mice. *Proc. Natl Acad. Sci. USA* 104, 2366–2371 (2007).
- Wu, J. et al. Beige adipocytes are a distinct type of thermogenic fat cell in mouse and human. Cell 150, 366–376 (2012).
- Petrovic, N. et al. Chronic peroxisome proliferator-activated receptor γ (PPARγ)
 activation of epididymally derived white adipocyte cultures reveals a population of
 thermogenically competent, UCP1-containing adipocytes molecularly distinct
 from classic brown adipocytes. J. Biol. Chem. 285, 7153–7164 (2010).
- Schulz, T. J. et al. Identification of inducible brown adipocyte progenitors residing in skeletal muscle and white fat. Proc. Natl Acad. Sci. USA 108, 143–148 (2011).
- 11. Tseng, Y. H. et al. New role of bone morphogenetic protein 7 in brown adipogenesis and energy expenditure. *Nature* **454**, 1000–1004 (2008).
- Whittle, A. J. et al. BMP8B increases brown adipose tissue thermogenesis through both central and peripheral actions. Cell 149, 871–885 (2012).



- Seale, P. et al. PRDM16 controls a brown fat/skeletal muscle switch. Nature 454, 961–967 (2008).
- Timmons, J. A. et al. Myogenic gene expression signature establishes that brown and white adipocytes originate from distinct cell lineages. *Proc. Natl Acad. Sci. USA* 104, 4401–4406 (2007).
- Atit, R. et al. β-catenin activation is necessary and sufficient to specify the dorsal dermal fate in the mouse. Dev. Biol. 296, 164–176 (2006).
- Lepper, C. & Fan, C. M. Inducible lineage tracing of Pax7-descendant cells reveals embryonic origin of adult satellite cells. Genesis 48, 424–436 (2010).
- Schmid, P., Lorenz, A., Hameister, H. & Montenarh, M. Expression of p53 during mouse embryogenesis. *Development* 113, 857–865 (1991).
- Sanchez-Gurmaches, J. et al. PTEN loss in the Myf5 lineage redistributes body fat and reveals subsets of white adipocytes that arise from Myf5 precursors. Cell Metab. 16, 348–362 (2012).
- Buckingham, M. E., Lyons, G. E., Ott, M. O. & Sassoon, D. A. Myogenesis in the mouse. Ciba Found. Symp. 165, 111–131 (1992).
- Kishigami, S. & Mishina, Y. BMP signaling and early embryonic patterning. Cytokine Growth Factor Rev. 16, 265–278 (2005).
- Gupta, R. K. et al. Transcriptional control of preadipocyte determination by Zfp423. Nature 464, 619–623 (2010).
- Farmer, S. R. Transcriptional control of adipocyte formation. Cell Metab. 4, 263–273 (2006).
- Cannon, B. & Nedergaard, J. Nonshivering thermogenesis and its adequate measurement in metabolic studies. J. Exp. Biol. 214, 242–253 (2011).
- 24. Fisher, F. M. et al. FGF21 regulates PGC-1α and browning of white adipose tissues in adaptive thermogenesis. Genes Dev. 26, 271–281 (2012).
- Boström, P. et al. A PGC1-α-dependent myokine that drives brown-fat-like development of white fat and thermogenesis. Nature 481, 463–468 (2012).
- Collins, S. β-Adrenoceptor signaling networks in adipocytes for recruiting stored fat and energy expenditure. Front. Endocrinol. 2, 102 (2011).
- Tseng, Y. H., Cypess, A. M. & Kahn, C. R. Cellular bioenergetics as a target for obesity therapy. Nature Rev. Drug Discov. 9, 465–482 (2010).
- Feldmann, H. M., Golozoubova, V., Cannon, B. & Nedergaard, J. UCP1 ablation induces obesity and abolishes diet-induced thermogenesis in mice exempt from thermal stress by living at thermoneutrality. *Cell Metab.* 9, 203–209 (2009).

- Rothwell, N. J. & Stock, M. J. Surgical removal of brown fat results in rapid and complete compensation by other depots. Am. J. Physiol. 257, R253–R258 (1989).
- 30. Xue, B. et al. Genetic variability affects the development of brown adipocytes in white fat but not in interscapular brown fat. J. Lipid Res. 48, 41–51 (2007).

Supplementary Information is available in the online version of the paper.

Acknowledgements This work was supported in part by National Institutes of Health (NIH) grants R01 DK077097 (Y.-H.T.), and Joslin Diabetes Center's Diabetes Research Center (DRC; P30 DK036836 from the NIDDK), a research grant from the Eli Lilly Research Foundation, and by funding from the Harvard Stem Cell Institute (to Y.-H.T.). T.J.S. was supported by the Mary K. lacocca Foundation and the German Research Foundation (DFG; SCHU2445/1-1). P.H. was supported by a Scientist Development Grant from the American Heart Association (0730285N). K.L.T. was supported by NIH fellowships (T32 DK007260 and F32 DK091996). R.X. was supported by Project 985III-YFX0302 and NSFC81070680 from the National Natural Science Foundation of China. The authors thank Stryker Regenerative Medicine for the gift of recombinant BMP7. We acknowledge V. Kaartinen, B. Kahn, K. Lyons and P. Soriano for providing floxed Acvr1 mice, FABP4-Cre mice, Bmpr1b heterozygous mice and Myf5-Cre mice, respectively. The authors thank C. R. Kahn, L. J. Goodyear, E. Kokkotou and D. Breault for comments on the manuscript. The authors wish to thank J. LaVecchio, G. Buruzula, A. Wakabayashi, A. Pinkhasov, A. Clermont, M. Mulvey, C. Cahill and G. Sankaranarayanan for technical assistance, and E. Caniano for editorial contributions.

Author Contributions T.J.S. and Y.-H.T. planned most of the experiments and wrote the paper. T.J.S. performed the majority of the experiments. P.H., T.L.H., L.E.M., R.X. and K.L.T. performed some of the animal and immunofluorescence experiments and/or provided research assistance. A.M.C. helped with the infrared thermography and provided valuable research materials. Y.M. and E.G. planned some of the experiments and contributed valuable research materials.

Author Information Reprints and permissions information is available at www.nature.com/reprints. The authors declare no competing financial interests. Readers are welcome to comment on the online version of the paper. Correspondence and requests for materials should be addressed to Y.-H.T. (yu-hua.tseng@joslin.harvard.edu).

METHODS

Animals. All animal procedures were approved by the Institutional Animal Use and Care Committee at Joslin Diabetes Center. Transgenic mice carrying floxed alleles for Acvr1 (ref. 31) or Bmpr1a (ref. 32) were used to generate conditional gene deletion mouse models by intercrossing with either Myf5- (ref. 33) or FABP4driven34 Cre expression as indicated. For studies involving Bmpr1b deletion, animals with whole-body gene deletion of this receptor were used³⁵. Myf5-Creexpressing animals were also crossed to Rosa26-YFP reporter mice (The Jackson Laboratory) in addition to the Bmpr1a-flox alleles for Myf5-lineage tracing and GFP labelling of Bmpr1a-deficient cells as described before¹⁰. For genotyping, DNA was isolated from tail tip biopsies by boiling in 0.5 ml 50 mM NaOH for 15 min, followed by neutralization by addition of 50 µl 1 M Tris-base (pH 6.8) and thorough vortexing. PCR genotyping was performed using primers as listed in Supplementary Table 1. Expected band sizes for Bmpr1a during gel analysis were 180 bp for the wild-type allele and 230 bp for the floxed allele. For recombination analysis of Bmpr1a mRNA, expected band sizes were 396 and 233 bp for the intact and recombined alleles, respectively, and 178 bp for the control PCR of exons 6 to 7. For Acvr1 genotyping, the PCR product was subsequently digested using the restriction enzyme Bgl-I (New England Biolabs) at 37 °C overnight, yielding a band at 250 bp for wild-type mice, and a double band at 90 bp and 160 bp for floxed alleles (all three bands in heterozygotes). Expected band sizes for Bmpr1b were 350 bp for the wild type, and 300 bp for the null allele. Expected band sizes for the Rosa26-YFP reporter mice were 600 bp for the wild-type allele and 320 bp for the mutant allele. For Myf5-Cre genotyping, bands at 600 and 400 bp for wild-type and mutant alleles, respectively, were expected. For a general Cre PCR, a single band at approximately 350 bp indicated presence of Cre cDNA in the genome. For loading control, IRS-1 primers were added for co-amplification in the same reaction (band at approximately 500 bp) to ensure proper loading with template DNA. To stimulate the browning of white adipose depots, mice were treated with daily intraperitoneal injections of 1 mg kg⁻¹ bodyweight CL-316,243 (Sigma-Aldrich) dissolved in PBS (also used for control injections) for up to 10 days. For experiments involving high-fat-diet feeding, 4- to 6-week-old animals were placed on a diet containing 45 or 60% kilocalories from fat (Research Diets). For cold exposure and thermoneutral conditions, animals were housed at 5 °C or 30 °C, respectively, for the indicated times in a controlled environmental chamber (Caron Products & Services) with free access to food and water. Body core temperature was determined by rectal probe measurements.

Haematoxylin and eosin staining. Sections were prepared, processed and stained as described¹¹.

Immunofluorescence. Sections were deparaffinized and prepared as described¹¹. Primary antibodies were incubated overnight at 4 °C: Ki67 (1:200, rabbit polyclonal; Abcam); UCP1 (1:50, rabbit polyclonal; AnaSpec), tyrosine hydroxylase (1:50, rabbit polyclonal; Millipore), GFP (1:200, goat polyclonal; Novus USA). After primary antibody incubation, the sections were washed and incubated with appropriate secondary antibody (Alexa Fluor-488 (green) or -594 (red); Invitrogen) at a 1:200 dilution for 10 min in the dark. After secondary antibody incubation, sections were washed with distilled water for DAPI staining (0.1 µg ml⁻¹ in water for 5–10 min in the dark), and mounted. Sections were kept in the dark after mounting and analysed by confocal microscopy on a Zeiss LSM-410 Invert Laser Scan Microscope (Carl Zeiss MicroImaging, Thornwood, NY), or using a fluorescence microscope (Olympus BX60F-3; Olympus Corporation). Quantification of tyrosine hydroxylase was performed by using the ImageJ software. Identical conditions and settings were used for picture acquisition and analysis. A threshold was set for each image to eliminate background and to create a binary mode image. A minimum particle size of 20 pixels was used as exclusion criteria to eliminate unspecific background and for quantification of areas that stained positive for tyrosine hydroxylase. For quantification of Ki67 staining, Ki67⁺ nuclei were counted in areas identified as BAT by microscopic inspection of morphology and comparison to published sources³⁶, and normalized to the total number of DAPI⁺ nuclei in the same area. For each section and animal, images from three representative areas were analysed.

TdT-mediated dUTP nick end staining (TUNEL assay). For detection of DNA fragmentation, sections were deparaffinized and blocked for autofluorescence as described¹0. Sections were blocked in 1% BSA, 0.5–1% Triton X-100 in PBS for 1 h, followed by washes in PBS. Terminal-strand labelling was performed for 1.5 h at 37 °C in TdT buffer (30 mM Tris-HCl, 140 mM Na-Cacodylate, 1 mM cobalt (II) chloride, pH 7.2) in the presence of dATP, biotinylated dUTP and terminal deoxynucleotidyl transferase (all from Roche Applied Science). The reaction was stopped by immersion in 2× SSC buffer and subsequent incubation with Cy3-labelled streptavidin (1:200; Jackson ImmunoResearch Laboratories) for 1 h in the dark. Sections were then stained with DAPI, mounted, and analysed as described earlier.

RNA and protein quantification. RNA extraction, cDNA synthesis, and quantitative real-time PCR (qPCR) were performed as described before¹¹. For qPCR

analysis, C_t values <30 were used for gene expression analysis. Protein detection by western blotting was performed as described before 11. Primary antibodies were incubated overnight at 4 °C: phospho-Smad-1/5/8 (1:1,000, rabbit polyclonal), SMAD1 (1:1,000, rabbit polyclonal), phospho-p38MAPK (1:1,000, rabbit polyclonal), p38MAPK (1:1,000, rabbit polyclonal) (all from Cell Signaling Technologies), UCP1 (1:500, goat polyclonal; Santa Cruz Biotechnology) and α -tubulin (1:8,000, mouse monoclonal; Sigma-Aldrich). HRP-coupled secondary antibodies (Cell Signaling Technologies) were used at 1:2,000 dilutions at room temperature for 2 h followed by detection using the ECL system.

Cell sorting. Sca1⁺ adipocyte progenitor cells were isolated from cBAT and sWAT of Myf5-BMPR1A-KO mice and control littermates, and differentiated as described before¹⁰.

Immortalized pre-adipocytes. Immortalized cell lines were generated as described previously³⁷. In brief, cBAT from individual newborn pups (P1 or P2) of homozygous floxed parents for the respective BMP receptor was collected and pre-adipocytes were isolated by enzymatic digestion. Pre-adipocytes were immortalized by infection with SV40-expressing lentivirus and subsequent selection with puromycin. Stable cell lines were then infected with adenovirus expressing either GFP (control) or a Cre::GFP fusion construct for *in vitro* recombination (Gene Transfer Vector Core, University of Iowa). Forty-eight hours after infection, GFP⁺ cells were collected by flow cytometry and expanded for subsequent use in experiments. DNA was isolated for PCR analysis to determine full recombination of the respective receptor gene using the primers as detailed earlier.

Cell culture. Pre-adipocyte cell lines were cultured as described before¹¹, except that 2% fetal bovine serum was used during differentiation. BMP7 treatments (3.3 nM) were performed for 3 days before 48 h of adipogenic induction, followed by a differentiation period of 5 days. Oil-Red-O staining was performed as described before¹¹.

Thermal imaging of skin-surface temperature. Measurement of skin temperature was performed using a thermal imaging camera (T300 InfraRed Camera; FLIR Systems). Skin-surface temperature of newborns was analysed using FLIR Reporter 8.5 software (FLIR Systems). Images were acquired by placing newborn mice of the same litter (P4–P6) in 6-well cell-culture dishes, and 2–3 images of each mouse from different angles were acquired to minimize temperature variations due to different postures of the animal. Software drawing tools were used to draw a region of interest (ROI) around the entire animal, and average body surface temperature was calculated using that ROI. For each animal, an average temperature value of the temperatures from all single images was calculated. These averages were then used for statistical analysis.

Serum parameters. Serum levels of noradrenaline were determined using a commercially available ELISA kit and according to the manufacturer's instructions (Norepinephrine (Research) ELISA; IBL America). To stabilize the noradrenaline, 1 mM EDTA and 4 mM sodium metabisulphite were added to the serum. Serum was prepared by spinning freshly collected blood in a cooled centrifuge at 6,000g for 20 min. The clear supernatant was collected and stored at $-80\,^{\circ}\text{C}$. Samples were analysed within 12 weeks after collection. To determine circulating irisin levels, a commercially available ELISA assay kit was used according to the manufacturer's specifications (Phoenix Pharmaceuticals).

Body composition. Relative contents of lean and fat mass were determined using dual-energy X-ray absorptiometry (DEXA) according to the manufacturer's instructions (GE Lunar PIXImus 2, General Electric Medical Systems). Animals were anaesthetized with pentobarbital (50 mg kg $^{-1}$, intraperitoneally) and placed in the scanning area to measure body composition. Relative lean and fat mass were calculated by normalizing to body weight.

Noradrenaline-induced thermogenic capacity. Measurement of maximum thermogenic capacity was performed as described before with some modifications^{12,28}. Animals were maintained in the cold as described earlier for 8 days before the experiment. All measurements were performed at room temperature. Oxygen consumption by indirect calorimetry was assessed using the Comprehensive Lab Animal Monitoring System (CLAMS; Columbus Instruments) and the Oxymax for Windows software (version 4.58) for data analysis. Animals were anaesthetized with pentobarbital (80 mg kg⁻¹, intraperitoneally), and indirect calorimetry was performed immediately for 30 min to record basal values of oxygen consumption. The sampling interval was set to 15 min to allow for stable oxygen consumption assessment throughout the experiment. After three data points were obtained, animals were briefly removed from the chamber and noradrenaline was injected subcutaneously (1 mg noradrenaline bitartrate per kg; Sigma-Aldrich), and oxygen consumption was recorded for another 90 min. To determine maximum noradrenaline-induced thermogenic capacity (ΔVO_2), the average value for basal oxygen consumption before noradrenaline injection was calculated and subtracted from the average value of highest noradrenalineinduced oxygen consumption (t_{60} and t_{75}). Areas under the curve (AUC) were calculated for the curves after noradrenaline injection. Data were presented either

not normalized, that is, per animal, or after normalization to total body weight, or total fat mass (from DEXA scan).

Denervation of cBAT. Denervation of cBAT was performed as described before³⁸. C57BL/6J mice (The Jackson Laboratory) aged 6 weeks were used for denervations. In brief, mice were anaesthetized and placed on a warm pad to maintain body temperature. Under a stereomicroscope, an incision was made posterior to the interscapular cBAT pad. Surrounding muscle and white fat was carefully moved to the side and the cBAT pad was turned upward to expose the five branches of the intercostal nerve bundles. Denervation was performed by isolating and cutting the nerve bundles and removing a portion of about 1–2 mm from each strand. Care was taken not to damage the adjacent blood vessels. The procedure was performed on left and right lobes of the interscapular brown fat. BAT pads, surrounding white fat, and muscle were placed in the original locations and the incision was closed using tissue adhesive glue (Vetbond, 3M Animal Care Products). The same procedure was performed for sham surgeries, except that nerve bundles were not cut. Animals were housed in single cages and monitored daily during the first week of recovery. After 10 weeks, animals were divided in four groups: (1) sham-operated mice receiving intraperitoneal vehicle injections (PBS); (2) sham-operated mice receiving injections of CL-316,243 as described earlier; (3) denervated mice receiving vehicle; or (4) CL-316,243.

Statistical analysis. All statistical analyses were performed using the programs Excel (Microsoft), Statview (SAS Institute) and GraphPad Prism (GraphPad

Software). Statistical analyses were performed using two-tailed Student's t-test or ANOVA for comparing the means of two or multiple groups, respectively. Nonparametric testing (U-Mann–Whitney test) was used where appropriate, that is, when normal distribution of sample sets was not evident. The means of two groups were considered significantly different when P < 0.05.

- Dudas, M., Sridurongrit, S., Nagy, A., Okazaki, K. & Kaartinen, V. Craniofacial defects in mice lacking BMP type I receptor Alk2 in neural crest cells. *Mech. Dev.* 121, 173–182 (2004).
- Mishina, Y., Hanks, M. C., Miura, S., Tallquist, M. D. & Behringer, R. R. Generation of Bmpr/Alk3 conditional knockout mice. Genesis 32, 69–72 (2002).
- Tallquist, M. D., Weismann, K. E., Hellstrom, M. & Soriano, P. Early myotome specification regulates PDGFA expression and axial skeleton development. Development 127, 5059–5070 (2000).
- Abel, E. D. et al. Adipose-selective targeting of the GLUT4 gene impairs insulin action in muscle and liver. Nature 409, 729–733 (2001).
- Yi, S. E., Daluiski, A., Pederson, R., Rosen, V. & Lyons, K. M. The type I BMP receptor BMPRIB is required for chondrogenesis in the mouse limb. *Development* 127, 621–630 (2000).
- 36. Kaufman, M. H. The Atlas of Mouse Development Vol. 1 (Academic, 1992).
- Klein, J., Fasshauer, M., Klein, H. H., Benito, M. & Kahn, C. R. Novel adipocyte lines from brown fat: a model system for the study of differentiation, energy metabolism, and insulin action. *Bioessays* 24, 382–388 (2002).
- Pulinilkunnil, T. et al. Adrenergic regulation of AMP-activated protein kinase in brown adipose tissue in vivo. J. Biol. Chem. 286, 8798–8809 (2011).